Hindawi
Mobile Information Systems
Volume 2022, Article ID 3104149, 14 pages
https://doi.org/10.1155/2022/3104149

Research Article

Optimal Control Strategy of Back-to-Back Converter Based on AC/DC Voltage Source Converter

Haotian Wu,[1,2] **Zhong Wei**,[1] **and Shiwen Liu**[3]

[1]*Shanghai Investigation, Design & Research Institute Co., Ltd, Shanghai 200335, China*
[2]*North China Electric Power University, Beijing 102206, China*
[3]*Shanghai University of Electric Power, Shanghai 200000, China*

Correspondence should be addressed to Haotian Wu; 50201603@ncepu.edu.cn

Received 20 April 2022; Revised 6 June 2022; Accepted 20 June 2022; Published 15 July 2022

Academic Editor: Gopal Chaudhary

The back-to-back converter is a converter system composed of two voltage source converters (VSC). Because VSC can regulate the output of active and reactive power, the back-to-back converter has a good dynamic and static performance. However, not all passive loads are three-phase symmetrical. The existing control strategy may lead to asymmetric output voltage when back-to-back converter is used to supply unbalance load. Usually, an inner loop d/q decoupling controller, a constant DC voltage controller of the rectifier side, and a constant AC voltage controller of the inverter side are established. In this article, in order to improve the rectifier side, fuzzy online self-tuning is used to increase PI parameters on the outer voltage loop. PI control is replaced by PR control on the inner current loop. The improved rectifier control can reduce the overshoot and the output of harmonics. For the inverter side, the three-phase voltage will be imbalanced. Therefore, using PR control, which can track a sinusoidal signal without steady-state error, the control strategy of inverter is changed into "outer loop constant voltage and PR control-inner loop current d/q decoupling control." This strategy can solve the unbalance problem of three-phase AC output. The simulation results show that the control strategy can solve the problem of asymmetric output voltage of the inverter side effectively.

1. Introduction

With the development of power electronics technology, AC\DC converter components have undergone a transition from a mercury arc valve to a thyristor. AC\DC converter includes line commuted converter (LCC) and voltage source converter (VSC). However, the traditional AC\DC LCC based on the phase-controlled commutation technology thyristor device has a low frequency and a large commutation loss. In addition, the traditional AC\DC LCC requires an external grid to provide a commutation voltage (i.e., a commutation short circuit ratio). Therefore, it cannot separately supply power to the passive network [1–3]. Different with LCC, VSC is a new high-voltage DC transmission with the modular design. It not only can improve the transmission capacity but also has the advantages of small energy loss, long transmission distance, and large capacity. In addition, it can supply power to the passive network separately [4, 5].

The back-to-back converter consists of two VSC components, so it has a good dynamic and static performance. It can control the active and reactive output through control strategy to improve power quality. In order to propose a suitable control strategy for implementing the primary control function of back-to-back converter, many scholars have studied the control strategy. In reference [6], MATLAB simulation model of back-to-back converter to the passive network is established to study the control strategies of the rectifier side and the inverter side. In reference [7], the influence of active load and reactive load on voltage and frequency is studied based on MATLAB simulation model of back-to-back converter supply to passive networks. In reference [8], the inverse system model of back-to-back converter is established by state feedback internalization. Based on the sliding mode variable structure control theory, a new type of controller that back-to-back converter supply to the passive network is established. However, the above research

is not systematic. This results in a control strategy and makes it difficult to solve multiple operational problems in the power system.

The existing research on the power supply of back-to-back converter to three-phase asymmetric passive network is mainly divided into two aspects. Firstly, different control strategies are usually used to control the output of the inverter to solve the asymmetry problem caused by the three-phase asymmetric load when the back-to-back converter supplies power to the load. Common control strategies include d/q instantaneous control and symmetrical component component control. Reference [9] is based on PR control to effectively track a sinusoidal signal at a certain frequency. PR control is introduced into the α/β coordinate system to achieve current balance control of the primary side three-phase current. After that, the imbalance problem of solving the three-phase output current is solved. Second, for the three-phase asymmetric output voltage, the two-phase α/β stationary coordinate system is used to dynamically compensate the three-phase voltage imbalance. In reference [10], the output voltage is separated by positive and negative order through second-order generalized integration. Further, the VUF-based voltage compensation reference generator corrects the reference voltage of the voltage loop. However, references [7–10] do not fully consider the influence of the control strategy of back-to-back converter including the rectifier side, which may lead to the problem of overshooting time and reaction time on the rectifier side and the asymmetry of the inverter output voltage.

In order to design the control strategy from the rectifier side to the inverter side when back-to-back converter supplies to the three-phase asymmetric passive network, this paper first analyzes the mathematical model of VSC in the d/q rotating coordinate system. A relational expression of active and reactive power on the AC side is obtained. On the basis of analyzing the common control strategies of the converter, the rectifier side fixed DC voltage controller and the inverter side fixed AC voltage controller are designed. For the rectifier side fixed DC voltage control, the voltage outer loop is improved by combining fuzzy control with PI control. At the same time, no static adjustment of the current is achieved by PR controller to improve the current inner loop. For the power transmission control problem caused by the three-phase unbalanced condition of the inverter side fixed AC voltage control load, the "constant AC voltage" single-loop control is changed to the "outer loop constant voltage-inner loop current decoupling" double closed-loop control. The three-phase distortion of the supply voltage is solved by using PR control to retrofit the voltage outer loop. The realization that back-to-back converter supplies power to unbalance load is realized.

2. Topology and Mathematical Model of AC/DC Voltage Source Converter

2.1. The Mathematical Model of VSC. The VSC topology diagram is shown in Figure 1.

According to the topology diagram of VSC and Kirchhoff voltage law, the mathematical model of three-phase PWM voltage source converter (VSC) in three-phase static coordinate system (a,b,c) is as follows:

$$\begin{cases} L\dfrac{\mathrm{d}i_a}{\mathrm{d}t} + Ri_a = u_{sa} - u_a, \\ L\dfrac{\mathrm{d}i_b}{\mathrm{d}t} + Ri_b = u_{sq} - u_b, \\ L\dfrac{\mathrm{d}i_c}{\mathrm{d}t} + Ri_c = u_{sc} - u_c, \\ C\dfrac{\mathrm{d}u_{dc}}{\mathrm{d}t} = i_{dc} - i_d. \end{cases} \tag{1}$$

Clarke transform (3/2 transform) is as follows:

$$\begin{bmatrix} i_\alpha \\ i_\beta \\ 0 \end{bmatrix} = \sqrt{\frac{2}{3}} \begin{bmatrix} 1 & -\dfrac{1}{2} & -\dfrac{1}{2} \\ 0 & \sqrt{\dfrac{3}{2}} & \sqrt{\dfrac{3}{2}} \\ \dfrac{1}{\sqrt{2}} & \dfrac{1}{\sqrt{2}} & \dfrac{1}{\sqrt{2}} \end{bmatrix} \begin{bmatrix} i_a \\ i_b \\ c \end{bmatrix} = C_{3s/2s} \begin{bmatrix} i_a \\ i_b \\ c \end{bmatrix}. \tag{2}$$

Park transformation (2/2 transform) is as follows:

$$\begin{aligned} \begin{bmatrix} i_d \\ i_q \end{bmatrix} &= \begin{bmatrix} \cos\theta & -\sin\theta \\ \sin\theta & \cos\theta \end{bmatrix}^{-1} \begin{bmatrix} i_\alpha \\ i_\beta \end{bmatrix} \\ &= \begin{bmatrix} \cos\theta & -\sin\theta \\ -\sin\theta & \cos\theta \end{bmatrix} \begin{bmatrix} i_\alpha \\ i_\beta \end{bmatrix} = C_{2s/2r} \begin{bmatrix} i_\alpha \\ i_\beta \end{bmatrix}. \end{aligned} \tag{3}$$

After Clarke and Park transformation, the mathematical model of three-phase PWM converter in d/q rotating coordinate system is obtained:

$$\begin{cases} L\dfrac{\mathrm{d}i_d}{\mathrm{d}t} + Ri_d - \omega Li_d = u_{sd} - u_d, \\ L\dfrac{\mathrm{d}i_q}{\mathrm{d}t} + Ri_q + \omega Li_d = u_{sq} - u_q, \\ C\dfrac{\mathrm{d}u_{\mathrm{dc}}}{\mathrm{d}t} = i_{dc} - i_d, \end{cases} \tag{4}$$

where u_{sd} and u_{sq} are d/q axis components of grid voltage, respectively; u_d and u_q are the d/q axis components of the three-phase voltage on the AC side of the converter, respectively; i_d and i_q are the d/q axis components of the three-phase current on the AC side of the converter, respectively; u_{dc} and i_{dc} are the DC side voltage and current of the converter, respectively; i_d is the outlet current of DC

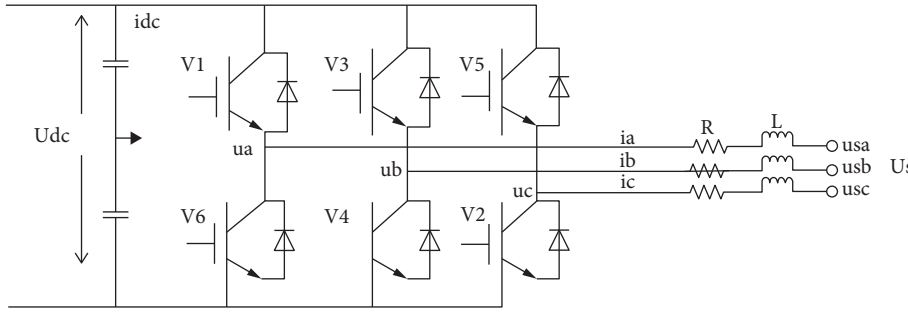

Figure 1: The topology diagram of VSC.

network; L is filter inductance; and C is the capacitance of DC side.

2.2. The Control Principle of VSC Power Decoupling. Under the condition of steady-state operation, ignoring the reactor resistance of VSC and the switching loss of VSC, the following can be obtained:

$$\begin{cases} u_d = u_{sd} + \omega L i_q, \\ u_q = -\omega L i_d. \end{cases} \tag{5}$$

In the d/q coordinate rotating system, the axis is oriented. At the same time, U_{sq} is 0 because the q-axis is 90 degrees ahead of the d-axis. According to the grid voltage orientation control strategy, the following equation can be obtained:

$$\begin{cases} U_{sd} = U_s, \\ U_{sq} = 0. \end{cases} \tag{6}$$

Combined with equations (5) and (6), the expressions of active power and the expressions of reactive power can be received based on the instantaneous power theory:

$$\begin{cases} P_{ac} = \dfrac{3}{2}\left(u_d i_d + u_q i_q\right) = \dfrac{3}{2} u_{sd} i_d = \dfrac{3}{2} u_s i_d, \\ Q_{ac} = \dfrac{3}{2}\left(u_{sq} i_d + u_{sd} i_q\right) = \dfrac{3}{2} u_{sd} i_q = -\dfrac{3}{2} u_s i_q. \end{cases} \tag{7}$$

From the above formula, u_s is invariant, and it can be obtained that the independent control of active power P_{ac} and reactive power Q_{ac} can be realized by controlling the value of i_d and i_q.

3. Design of Back-to-Back Converter to Three-Phase Passive Network Power Supply Controller

3.1. System Structure and Control Strategy Analysis of Back-to-Back Converter Power Supply to Three-Phase Passive Network. The structure diagram of back-to-back converter supplying power to the three-phase load is shown in Figure 2. The commutating reactor L_1 is used for the exchange of VSC energy on the rectifier side and filters out some higher harmonics. Capacitors C_1 and C_2 provide the voltage support required for the DC terminal and serve as an inrush current when the buffer arm is turned off. The role of higher harmonics on the DC side is reduced. The inverter side supplies power to the asymmetric load through a single resonant phase. For the characteristics of the whole system, the controllers on the rectifier side and the inverter side are designed separately [11].

The common control strategies of VSC converter station are generally divided into four types: (1) constant DC voltage control mode; (2) fixed active power control mode; (3) constant AC voltage control; and (4) variable frequency control mode. Different from the back-to-back converter supplying power to the normal three-phase passive network, the back-to-back converter supplies power to the three-phase asymmetric passive network. To maintain the stable operation of the whole system, the two main problems need to be solved: (1) the DC voltage of the DC channel is stable and (2) the inverter side a stable output of the AC voltage.

For the first problem, the stability of the DC voltage of the DC channel must be realized by the rectifier side. Therefore, the rectifier side VSC adopts the "outer loop fixed DC voltage-inner loop current decoupling" double closed-loop control mode. The outer loop realizes the fixed DC voltage control target. The inner loop current quickly tracks the reference current input from the outer loop. Then, the current waveform and phase control of the AC side of the inverter will be realized [12, 13]. For the second problem, the stable output of the AC voltage on the inverter side, due to the unbalanced output of the AC voltage caused by the three-phase asymmetric passive network, the traditional constant AC voltage control can no longer meet the needs. In this paper, PR control can track the sinusoidal signal without static difference. And the inverter VSC "fixed AC voltage single-loop control" is changed to "outer loop constant voltage PR control-inner loop current d/p decoupling control." The three-phase AC voltage on the inverter side remains unchanged regardless of how the three-phase asymmetric passive network changes [14, 15].

3.2. Current Inner Loop d/q Decoupling Controller Design. The mathematical model of the three-phase PWM AC/DC converter in the d/q rotating coordinate system shows that there are coupling terms $\omega L i_d$ and $\omega L i_q$. Using the input and output linearization control method [16], set

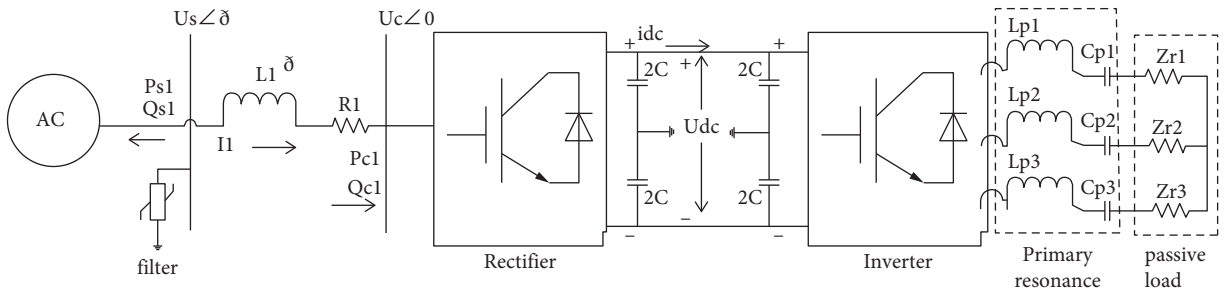

Figure 2: Block diagram of for back-to-back converter to supply a three-phase passive network.

$$\begin{cases} L\dfrac{\mathrm{d}i_d}{\mathrm{d}t} + Ri_d = \Delta u_d, \\ \\ L\dfrac{\mathrm{d}i_q}{\mathrm{d}t} + Ri_q = \Delta u_q. \end{cases} \tag{8}$$

Set $\triangle u_d$ and $\triangle u_p$ as follows, respectively:

$$\begin{cases} \Delta u_{\mathrm{d}} = K_p\left(i_d^* - i_d\right) + K_i\dfrac{\mathrm{d}\left(i_d^* - i_d\right)}{\mathrm{d}t}, \\ \\ \Delta u_q = K_p\left(i_q^* - i_q\right) + K_i\dfrac{\mathrm{d}\left(i_q^* - i_q\right)}{\mathrm{d}t}. \end{cases} \tag{9}$$

Equation (9) is subjected to the Laplace transform under zero initial conditions, and the PI controller expression can be obtained:

$$\begin{cases} \Delta u_d\left(K_p + \dfrac{K_i}{s}\right)\left(i_d^* - i_d\right), \\ \\ \Delta u_q\left(K_p + \dfrac{K_i}{s}\right)\left(i_q^* - i_q\right). \end{cases} \tag{10}$$

The simultaneous (8)–(10) can be obtained:

$$\begin{cases} \left(K_p + \dfrac{K_i}{s}\right)\left(i_d^* - i_d\right) = \Delta u_d = L\dfrac{\mathrm{d}i_d}{\mathrm{d}t} + Ri_d, \\ \\ \left(K_p + \dfrac{K_i}{s}\right)\left(i_q^* - i_q\right) = \Delta u_q = L\dfrac{\mathrm{d}i_q}{\mathrm{d}t} + Ri_q. \end{cases} \tag{11}$$

According to equation (4), the mathematical model of the three-phase PWM AC/DC converter in the d/q rotating coordinate system is as follows:

$$\begin{cases} L\dfrac{\mathrm{d}i_{\mathrm{d}}}{\mathrm{d}x} + Ri_d - \omega Li_q = u_{sd} - u_d, \\ \\ L\dfrac{\mathrm{d}i_{\mathrm{d}}}{\mathrm{d}t} + Ri_q - \omega Li_q = u_{sq} - u_q, \\ \\ C\dfrac{\mathrm{d}u_{\mathrm{dc}}}{\mathrm{d}t} + i_{dc} - i_d. \end{cases} \tag{12}$$

By combining equations (4) and (11), the d/q decoupling control expression based on current state feedback and voltage feed forward compensation can be obtained as follows [16, 17]:

$$\begin{cases} u_d = u_{sd} - \left(K_p + \dfrac{K_i}{s}\right)\left(i_d^* - i_d^*\right) + \omega Li_q, \\ \\ u_q = u_{sq} - \left(K_p + \dfrac{K_i}{s}\right)\left(i_q^* - i_q\right) + \omega Li_d. \end{cases} \tag{13}$$

The block diagram of the inner loop current decoupling controller is shown in Figure 3.

According to the controller designed in Figure 3, the size control of u_d and u_q can be control, and the decoupling between i_d and i_q can be realized [17].

3.3. Voltage Outer Loop Control of Rectifier Side VSC Based on Fuzzy PI Self-Tuning. Introducing fuzzy control into PI controller, a fuzzy PI self-tuning algorithm is formed. In fuzzy PI control, the proportional coefficient P and integral coefficient I change with the change of external factors, so fuzzy PI control is a kind of nonlinear control. The fuzzy PI control algorithm fully combines the respective advantages of conventional PI control and fuzzy control. It can adjust the proportional coefficient P and integral coefficient I in real time according to the actual changes of the outside world. Compared with the traditional PI control, it has better control effect and control accuracy. The schematic diagram of fuzzy PI control is shown in Figure 4 [18].

For fuzzy PI control algorithm, the control algorithm includes two inputs (e ec) and two outputs ($\triangle k_p$, $\triangle k_i$), which is the system error, ec is the error change rate, $\triangle k_p$ is the proportional coefficient variable output, and $\triangle k_i$ is the integral coefficient variable output. The universe on fuzzy sets is defined as follows: {−6, −5, −4, −3, −2, −1, 0, 1, 2, 3, 4, 5, 6}. e, ec, $\triangle k_p$, and $\triangle k_i$ are the four fuzzy subsets. Let e, ec, $\triangle k_p$, and $\triangle k_i$ obey the membership function curve distribution of triangle {NB, NM, NS, ZO, PS, PM, PB}, as shown in Figure 5.

The fuzzy membership control model is based on the fuzzy membership set and the fuzzy control rule table. Then, finding optimal PI parameter value is used to implement online self-tuning of PI parameter.

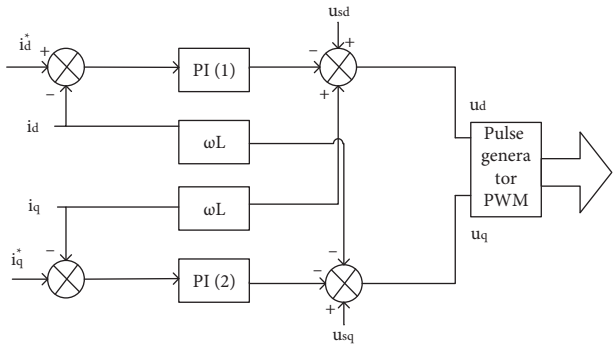

Figure 3: Current inner loop decoupling control diagram.

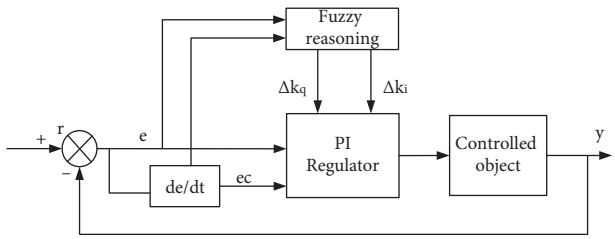

Figure 4: Block diagram of the fuzzy PI control.

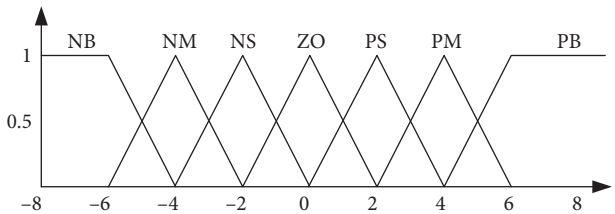

Figure 5: The curve of triangular membership function.

$$\left(\begin{cases} k_p = |k_p' + \Delta k_p \\ k_i = k_i' + \Delta k_i \end{cases} \right), \tag{14}$$

where $\triangle k_p$ is the proportional gain variation of fuzzy PI self-tuning; $\triangle k_i$ is the integral gain variation of fuzzy PI self-tuning; k_p' is the proportional gain setting value of fuzzy PI self-tuning; and k_i' is the integral gain setting value of fuzzy PI self-tuning.

In fuzzy PI controller, e is $(i_d^* - i_d)$ and ec is $(d(i_d^* - i_d)/dt, d(q_d^* - i_q)/dt)$. The error e and the rate of change ec of the error are both two-dimensional variables. Therefore, the fuzzy controller is a controller with a four-dimensional variable input and a two-dimensional variable ($\triangle k_p$ and $\triangle k_i$) output.

3.4. Improved Current Inner Loop Control for Rectifier Side VSC Based on PR Control. The principle of PR control: in thedouble closed-loop control system of AC grid connection of permanent magnet fan, the control objectives of voltage outer loop and current inner loop are different. The control goal of the current inner loop is to quickly track the current command and make the control system have good dynamic characteristics. Although the traditional PI control algorithm is relatively simple and reliable, its control effect is not ideal in the actual operation process, which is embodied in the following aspects: (1) if traditional PI control is adopted in the current inner loop, park transformation and Clarke transformation are required for the control quantity, and a large number of coordinate transformations will make the current inner loop control more complex; (2) when using traditional PI control, if you want to realize the decoupling of active and reactive power, it is necessary to introduce feed forward compensation ωLi_d and ωLi_q. In the actual operation process, the parameter of ωLi_d and the parameter of ωLi_q are related to temperature and they are not fixed values; and (3) the proportional coefficient and integral coefficient of traditional PI control are fixed values. In the process of current inner loop control, if the decoupling is not accurate, the control accuracy will be reduced.

Therefore, proportional resonance control PR is essentially PI control in two-phase d/q rotating coordinate system. Introducing the PR control algorithm into current inner loop control can not only reduce a lot of coordinate transformation but also omit feed forward compensation ωLi_d and ωLi_q, without power decoupling. Therefore, by introducing PR control, the current inner loop control at the network side can better achieve the control goal, quickly track the current command, and achieve no static error regulation. The control principle of proportional resonance PR is shown in Figure 6.

PR controller consists of a proportional link and a generalized integral link. The transfer function is as follows:

$$G_{pr}(s) = k_p + \frac{2k_i s}{s^2 + \omega_0^2}, \tag{15}$$

where k_p, k_i, and ω_0 are the proportional coefficient, integral coefficient, and the resonant frequency, respectively. It can be seen from the above formula that the gain of the ideal PR control at the resonant frequency ω_0 is infinite, while the gain at other frequencies is almost zero.

In the network side current inner loop control based on traditional PI control, the output power of three-phase PWM inverter is determined by the given current value $i_d^*$and i_q^*, in which the size of i_d^* determines the output of active power and the size of i_q^* determines the output of reactive power. At the same time, the two-cross compensation $\omega Li_d/\omega Li_q$ and the grid voltage E also affect the stability of the current inner loop control, but in practical engineering, the cross-coupling compensation $\omega Li_d/\omega Li_q$ will change with the change of external temperature, which is not a stable value. The current inner loop control based on the improved PR control in this paper is mainly divided into the following five steps: (1) the detection device is used to detect the AC current signal i_{abc} on the three-phase AC network side; (2) Clarke transform of i_{abc} will be performed to obtain i_α and i_β; (3) Park transforms the signal given by the voltage outer loop to obtain the given value i_α^* and i_β^* of the current inner loop; (4) the difference is made between i_α^*

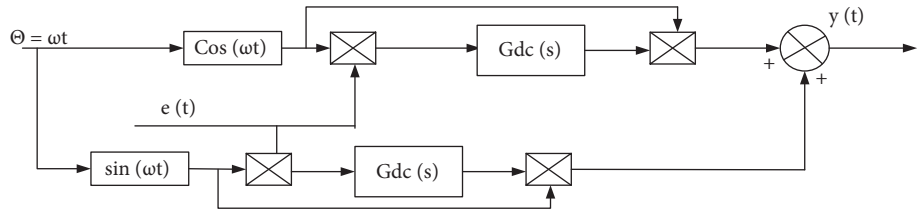

Figure 6: The principle diagram of PR control.

and i_α, i_β^* and i_β, and the two differences are used as the input of PR controller; and (5) the output of PR controller is used as the control command to control the six converter bridge arms of three-phase PWM inverter through SVPWM pulse width modulation.

Compared with traditional PI control, PR control has the following two advantages in the inner loop control of grid side current: (1) PR control only needs Clarke transformation of the control quantity, which reduces the complex operation of rotating coordinate system and the difficulty of control algorithm; (2) no cross-coupling compensation $\omega Li_d/\omega Li_q$ and Grid voltage E vector orientation are required, and the feed forward decoupling control is eliminated. Therefore, the changes of circuit parameters and grid voltage will not affect the accuracy of the control system, and the robustness and stability of the system will be greatly improved.

3.5. Rectifier Side Controller Design. To sum up, based on the double closed-loop decoupling control strategy of grid voltage vector orientation, the control of VSC on the rectifier side is deceptively transformed, and the control strategy of VSC on the rectifier side is established in this chapter. Among them, traditional PI control is transformed into fuzzy self-tuning PI control, which can adjust the proportional coefficient P and integral coefficient I in real time according to the changes of the outside world; AC current is the core of inner loop control. The goal of inner loop control is to track the grid voltage and maintain the same frequency and phase. Traditional PI control is transformed into PR control, which reduces the complex operation of rotating coordinate system, eliminates feed forward decoupling control and grid voltage vector orientation, and improves the stability and anti-interference ability of the system. The integral control diagram of VSC on the rectifier side in this chapter is shown in Figure 7.

3.6. Design of Inverter Side Controller. Back-to-back converter is connected to a passive network, in which case a single-loop constant AC voltage control is required.

The inverter three-phase AC voltage measurement u_{abc} is converted by d/q coordinates. The measured value is compared with the AC voltage reference value in the d/q coordinate system. U_d, u_q, and u_0 are obtained through the PI regulator. Finally, the resulting PWM control signal allows the converter to be adjusted. The inverter side fixed AC voltage control block diagram is shown in Figure 8.

3.7. Characteristic Analysis of Output Voltage Distortion under Unbalanced Load. Under three-phase unbalanced conditions, the distorted three-phase AC voltage can be expressed by three quantities: positive sequence voltage U_f^+, negative sequence voltage U_f^-, and zero-sequence voltage U_f^0.

$$\begin{cases} U_f = U_f^+ + U_f^0 + U_f^-, \\ \begin{bmatrix} u_a \\ u_b \\ u_c \end{bmatrix} = U_{fp}^+ \begin{bmatrix} \cos\left(\omega_b t + \varphi^+\right) \\ \cos\left(\omega_b t + \varphi^- + \dfrac{2\pi}{3}\right) \\ \cos\left(\omega_b t + \varphi^+ + \dfrac{2\pi}{3}\right) \end{bmatrix} \\ + U_{fp}^- \begin{bmatrix} \cos\left(\omega_b t + \varphi^-\right) \\ \cos\left(\omega_b t + \varphi^- + \dfrac{2\pi}{3}\right) \\ \cos\left(\omega_b t + \varphi^- + \dfrac{2\pi}{3}\right) \end{bmatrix} + U_{fp}^0 \begin{bmatrix} \cos\left(\omega_b t + \varphi^0\right) \\ \cos\left(\omega_b t + \varphi^0\right) \\ \cos\left(\omega_b t + \varphi^0\right) \end{bmatrix}, \end{cases} \tag{16}$$

where the positive, negative, and zero order electromotive force peaks are U_{fp}^+, U_{fp}^-, and U_{fp}^0, respectively; the initial phase angle of the fundamental voltage under positive sequence, negative sequence, and zero sequence are φ^+, φ^-, and φ^0, respectively.

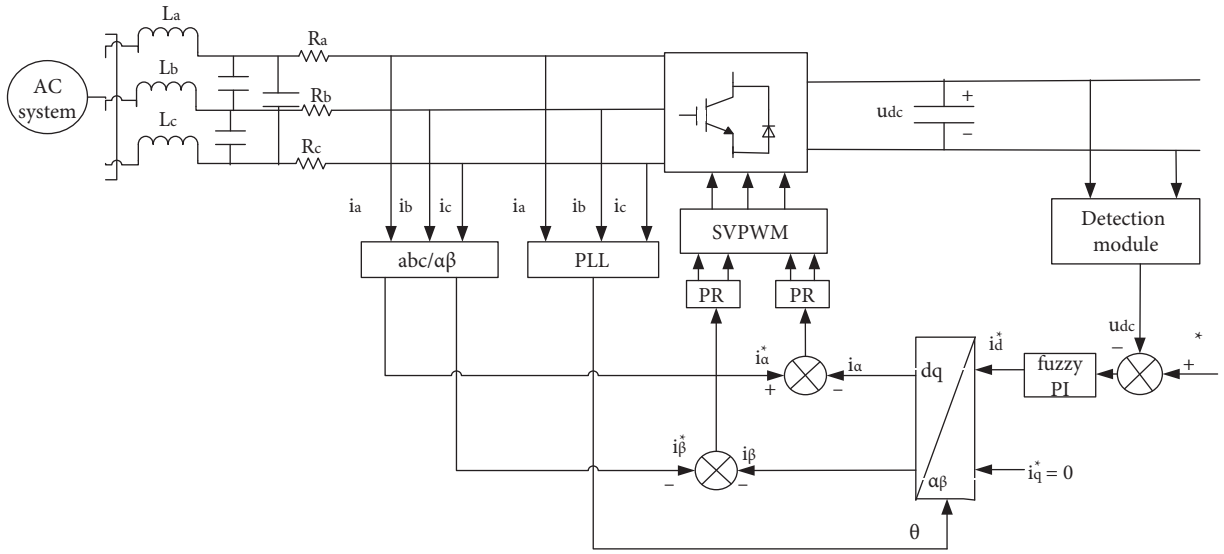

Figure 7: Integral control diagram of the rectifier side.

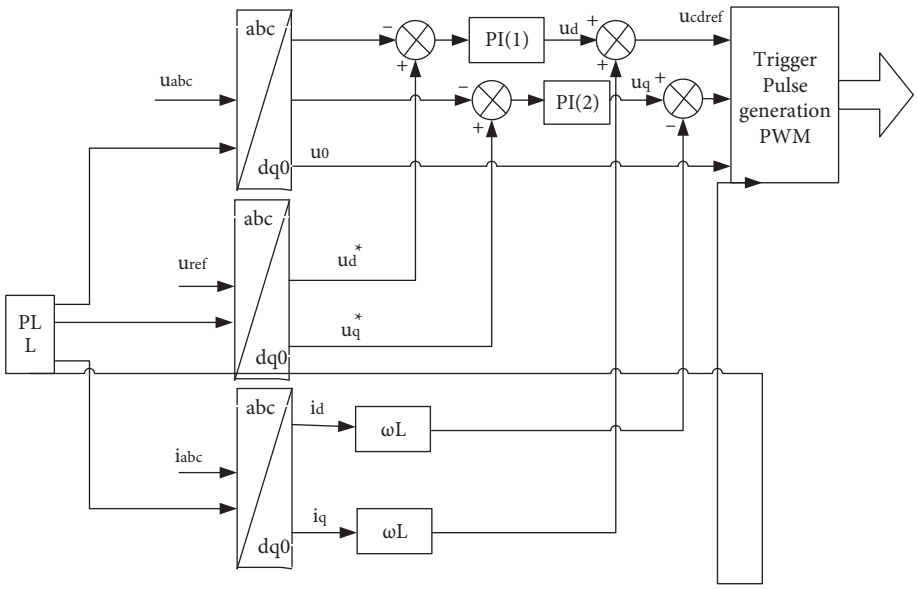

Figure 8: Common control diagram of the inverter side.

Since the three-phase inverter generally has no neutral connection, the zero-sequence electromotive force can be ignored. This means $U_{fp}^{0} = 0$. Then, equation (16) can be changed to

$$\begin{cases} U_f = U_f^+ + U_f^0 + U_f^-, \\ \begin{bmatrix} u_a \\ u_b \\ u_c \end{bmatrix} = U_{fp}^+ \begin{bmatrix} \cos\left(\omega_b t + \varphi^+\right) \\ \cos\left(\omega_b t + \varphi^- + \dfrac{2\pi}{3}\right) \\ \cos\left(\omega_b t + \varphi^+ + \dfrac{2\pi}{3}\right) \end{bmatrix} + U_{fp}^- \begin{bmatrix} \cos\left(\omega_b t + \varphi^-\right) \\ \cos\left(\omega_b t + \varphi^- + \dfrac{2\pi}{3}\right) \\ \cos\left(\omega_b t + \varphi^- + \dfrac{2\pi}{3}\right) \end{bmatrix}. \end{cases} \tag{17}$$

It can be seen from equation (17) that when the alternating current is three-phase distorted, both the positive sequence and the negative sequence need to consider the fundamental wave amount of the alternating voltage. As can be seen from the analytical equation (15), PR control has only a high gain at all and a large attenuation at other frequencies. No static tracking can be achieved when the system gains near infinity at the frequency point. Traditional PR control has only one frequency point. Therefore, the controller is overly sensitive to the signal frequency. However, in practical applications, in order to increase system bandwidth and improve stability, PR controller can be improved to

$$G_{pr}(s) = k_p + k_i \frac{2\omega_c s}{s^2 + 2\omega_c s + \omega_0^2}, \tag{18}$$

where ω_c is the cutoff frequency, $K_i = 100$, and $\omega_0 = 314$ rad/s. When $\omega_c = 2$ rad/s and 20 rad/s, the improved PR controller Bode diagram is shown in Figure 9.

It can be seen from the analysis of equation (18) and Figure 9 that the frequency response of PR controller is improved by ω_c. PR controller can simultaneously achieve high gain on both sides $\omega_c - \omega_0$ and $\omega_c - \omega_0$. This is equivalent to performing PI control in both positive and negative sequence coordinates. Therefore, PR control can realize the nonstationary tracking of the three-phase AC quantity and the correction of the three-phase distorted AC quantity.

3.8. Improved Voltage Loop Design of PR Controller. To illustrate the principle of PR control and d/q decoupling control, the voltage loop α axis is taken as an example for analysis. Its total transfer function is shown in Figure 10 [19].

The three-phase supply voltage u_{abc} and the given three-phase voltage u^*_{abc} are u_α and u^*_α obtained by Park transformation. The difference between these two gets the given output by the transfer function of PR controller$G_{PR}(s)$, the transfer function of the PWM link $G_{PWM}(s)$, and the transfer function of the resonant link $G_o(s)$ (including the load impedance). Set K_s as the amplification factor of the PWM device. T_S and T are the delay time and switching period of the PWM device, respectively. In addition, $T_s < T$. Normally the PWM switching frequency is large, so the time constant T_S is small. PWM device can be simplified to first-order inertia link $G_{PWM}(s) = K_S/T_S S + 1$. It can be obtained that the transfer function of the resonant link is $G_o(s) = 1/L_s + 1/C_s + Z_{r1}$.

The transfer function of the α-axis of the entire voltage flow control loop is as follows:

$$u_\alpha = \frac{G_{PR}(s)G_{PWM}(s)G_0(s)}{1 + G_{PR}(s)G_{PWM}(s)G_0(s)} u^*_\alpha. \tag{19}$$

It can be obtained from equation (19) that when the inverter operates at the specified power resonance point, $G_o(s)$ approximates infinity.$G_{PR}(s)G_{PWM}(s)G_0(s)$ is much larger than 1. Therefore, $(u_\alpha G_{PR}(s)G_{\mathrm{PWM}}(s)G_0(s)/1+ G_{PR}(s)G_{PWM}(s)G_0(s)u^*_\alpha)$.

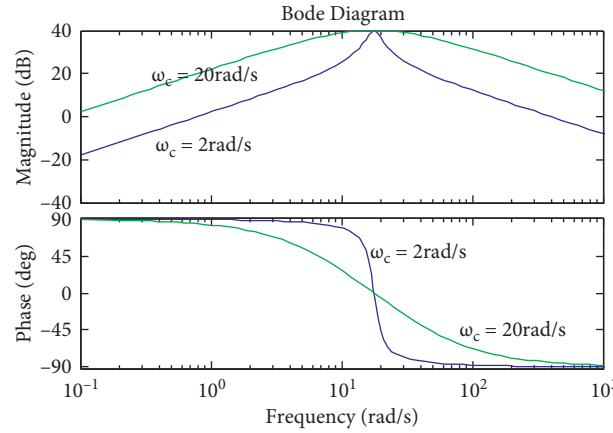

Figure 9: Bode graph of the improved PR controller.

Figure 10: Current loop transfer function with PR controller.

3.9. Design of VSC Controller for Inverting Side Power Supply to Three-Phase Unbalanced Load. The passive load is a three-phase asymmetry. Therefore, on the basis of analyzing the traditional double-loop control strategy, the traditional "fixed AC voltage single-loop control" can be modified by using PR control to track the characteristics of the sinusoidal signal without static difference. When back-to-back converter supplies power to the three-phase asymmetric load, the problem of the AC voltage distortion on the inverter side is solved.

From the 3.8 summary analysis, PR control can perform no static tracking for a specific three-phase AC signal. For the distorted three-phase AC voltage, if PR control is introduced in the control, the traditional vector-controlled three-phase AC voltage is converted to the two-phase stationary coordinate system, and the primary resonance frequency is set to the PR-controlled resonant frequency, the three-phase AC voltage without the static difference tracking of the command signal will be realized. Finally, the distortion of the three-phase AC voltage is corrected, and the symmetry and stability of the three-phase AC voltage on the inverter side are realized.

According to the above control target and control strategy analysis, the traditional inverter side fixed AC voltage single-loop control is changed to "outer loop fixed AC voltage-inner loop current decoupling" double closed-loop control. Further, the external loop using PR control voltage was modified. The stable power supply of back-to-back converter to the three-phase asymmetric passive network is realized. The overall control block diagram of the inverter side is shown in Figure 11.

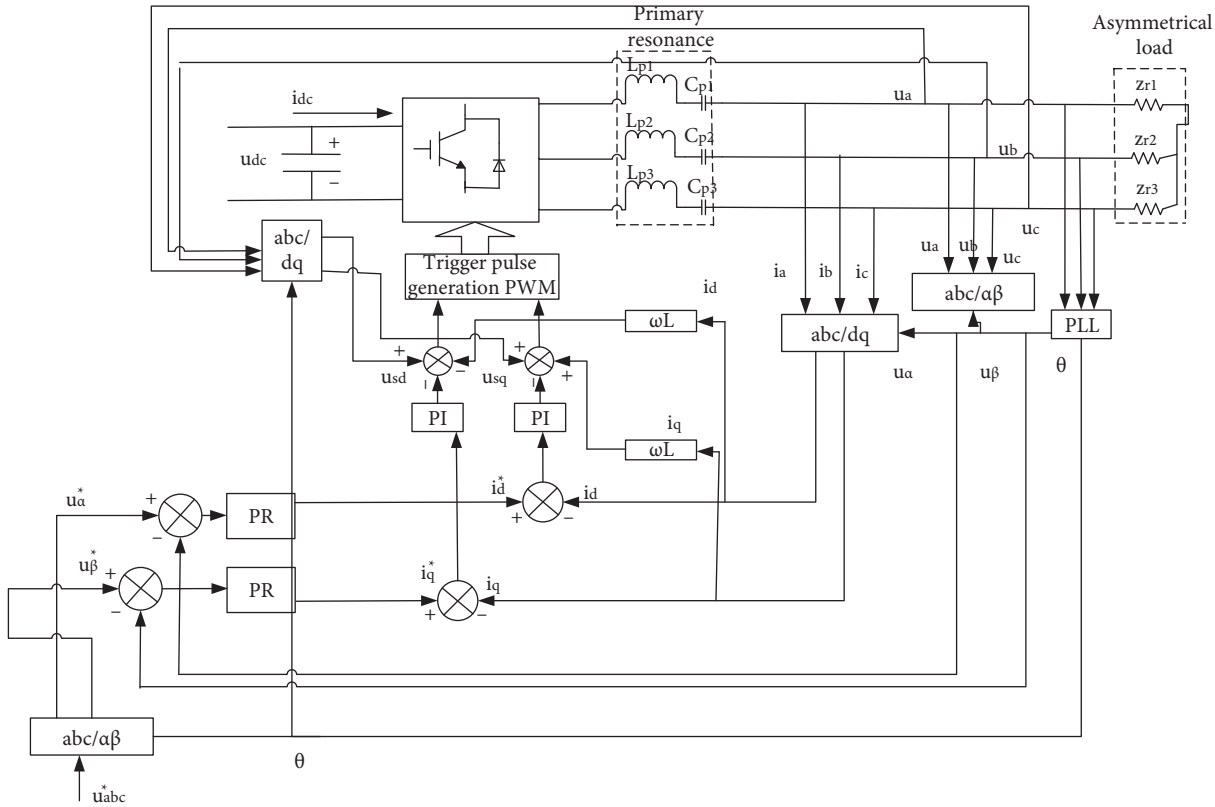

Figure 11: Integral control diagram of inverter side of back-to-back converter.

4. Simulation and Experimental Verification Based on MATLAB/SIMULINK

4.1. Simulation Model and Related Parameters. In this paper, the simulation model of back-to-back converter to three-phase asymmetric load is built by using MTALAB/SIMULINK simulation software. In the simulation model, the relevant control parameters of the rectifier side, the DC side, and the inverter side of back-to-back converter are given in Tables 1–3, respectively.

4.2. Rectification Side Simulation Results and Analysis. The voltage of the rectification side AC system is set to 15 kV/50 Hz and 20 kV/50 Hz, respectively, and the overshoot and reaction time of the AC-DC output signal (DC voltage) are observed.

SIMULINK simulation is performed on the rectification side using the conventional fixed DC voltage double closed-loop control, and the results are shown in Figures 12 and 13.

Fuzzy PI controller is used to improve the voltage outer loop of the conventional rectifier side double closed-loop control. PR controller is further used to improve the inner loop d/q decoupling controller. The simulation results of SIMULINK are shown in Figures 14 and 15.

The result comparison is divided into two parts. (1) In Figures 12 and 13, under the conventional PI control, U_{abc} takes different values from 15 KV to 20 KV; (2) In Figures 14 and 15, under the improved fuzzy PI control, U_{abc} takes different values from 15 KV to 20 KV.

Table 1: Related parameters of the rectifier side.

Parameters	Value
Rectification side AC system parameters	15 kV/3GVA/50 Hz 20 kV/3GVA/50 Hz
Inverter rated capacity	50 MW
Low pass filter LC parameters	5mH + 180 μF
PWM switching frequency	2 kHZ
Modulation	SPWM
Voltage outer loop Kp, Ki	0.015,1.6
Current inner loop Kp, Ki	5,15

Table 2: Related parameters of the DC side.

Parameters	Value
DC line length	10 km
Line resistance	0.015 Ω/km
Inductance	0.792mH/km
DC capacitor	30 mF
DC line capacitance	0.0144 μF

Comparing the two parts 1 and 2, it can be seen that the double closed-loop control of the rectifier improved by fuzzy PI control and PR control can change the PI parameters in real time according to external conditions. Compared with the first part 1, the part 2 has the following characteristics: the DC side voltage, the AC side active power, the AC side reactive power reaching the steady state, and the time taken for the steady state is small; the curve fluctuation is small; the anti-interference ability is stronger; the amount is also

Table 3: Related parameters of the inverter side.

DC side voltage	20 KV
Inverter rated capacity	50 MW
Primary resonant inductor	5 mH
Primary resonant capacitor	25.3 μF
Three-phase load resistor	84 Ω/50 Ω/24 Ω
Resonant frequency	1 kHZ
PWM switching frequency	2 kHZ
Modulation	SVPWM
Current inner loop kp, ki	0.4,500
Voltage outer loop kp, Kr	5,300
Three-phase parallel load after 0.35s	50 Ω

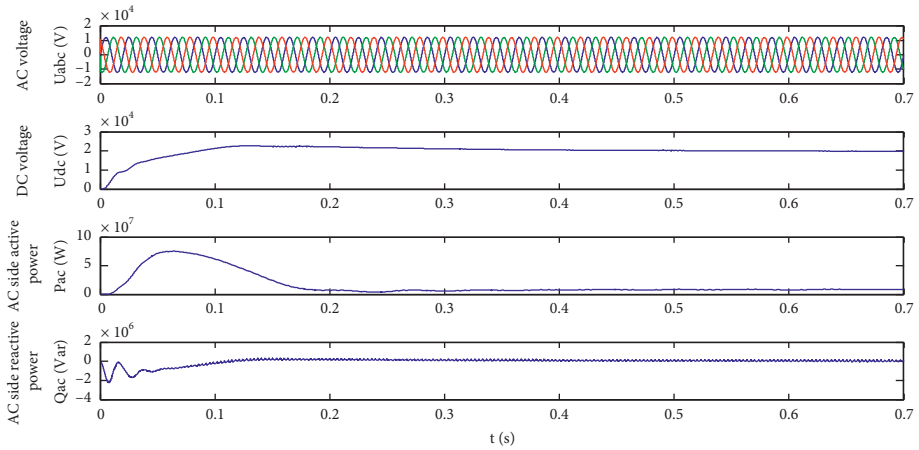

Figure 12: Simulation results of the common rectifier side when AC voltage is 15 KV.

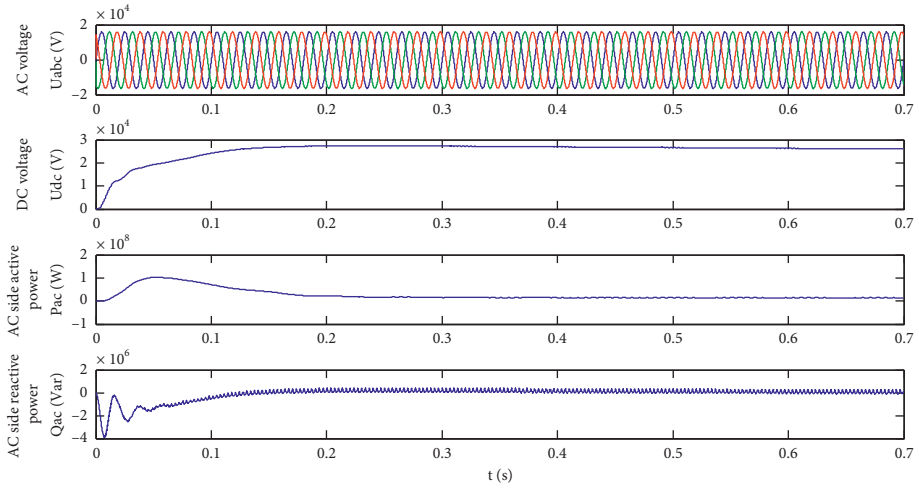

Figure 13: Simulation results of the common rectifier side when AC voltage is 20 KV.

smaller; the DC voltage can be stabilized earlier and faster. The control performance of the improved rectifier through fuzzy PI control and PR control has been significantly improved.

4.3. Inverter Side Simulation Results and Analysis of Back-to-Back Converter Powered to Three-Phase Asymmetric Passive Network. The control mode usually adopted for the inverter side that supplies power to the passive network is constant AC voltage single-loop control. This article mainly considers the case of supplying power to a three-phase asymmetric passive network. The three-phase asymmetric passive load affects the stable transmission of the three-phase alternating current on the inverter side. In this case, distortion of the three-phase AC voltage on the inverter side affects the stability of the AC voltage. In this paper, the double closed-loop control strategy

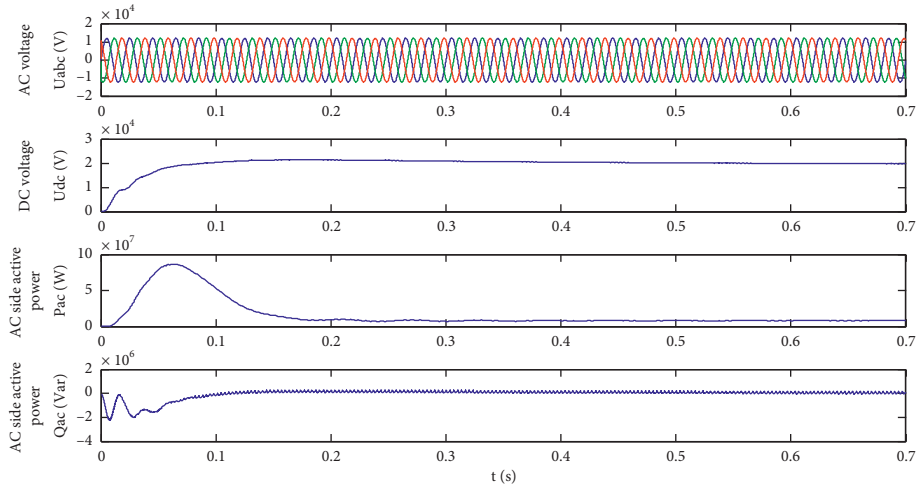

Figure 14: Simulation results of the improved rectifier side when AC voltage is 15 KV.

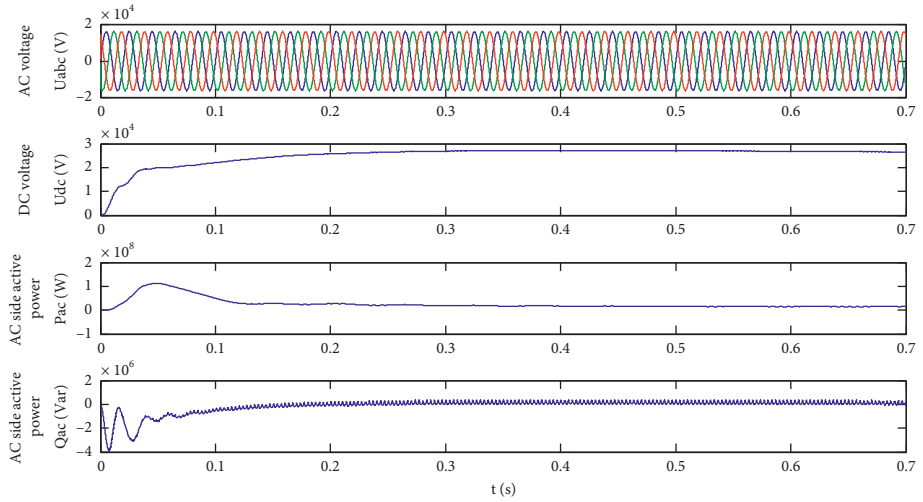

Figure 15: Simulation results of the improved rectifier side when AC voltage is 20 KV.

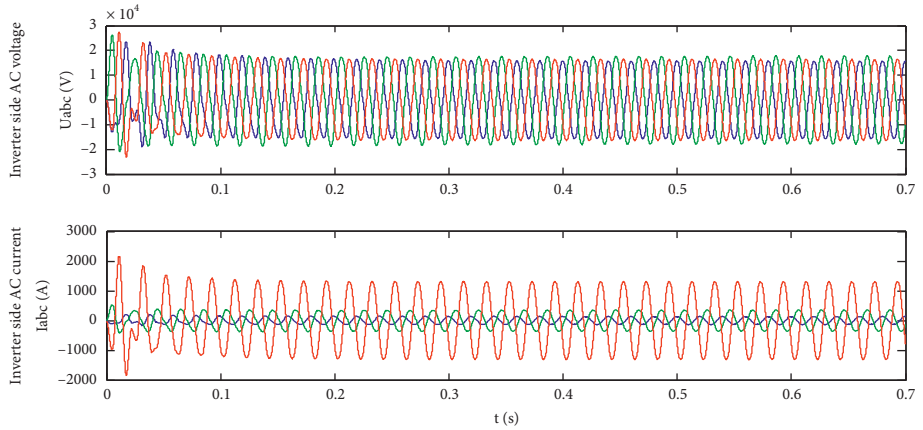

Figure 16: Simulation results of the common inverter side.

of "outer loop fixed AC voltage-inner loop current decoupling" is adopted. By using PR control to perform sinusoidal voltage signal without static tracking, the three-phase voltage imbalance problem generated by the asymmetric load is solved. The overall control objective is to control the AC side output and stabilize the three-phase AC

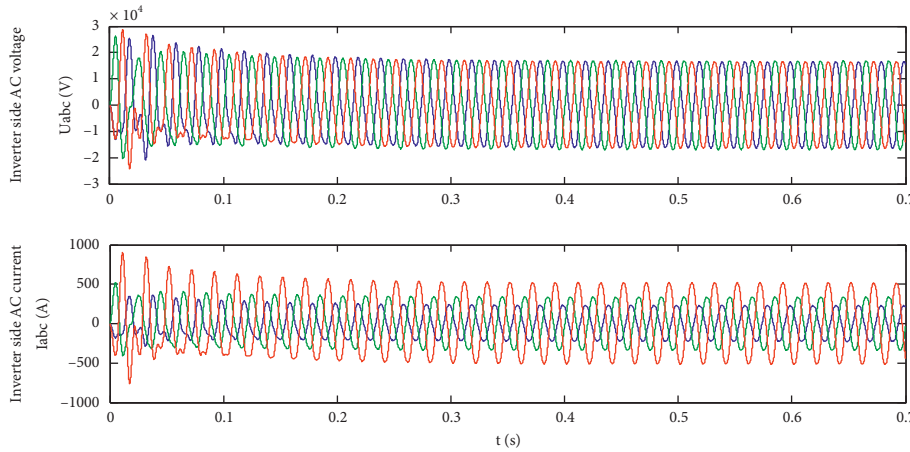

Figure 17: Simulation results of the improved inverter side.

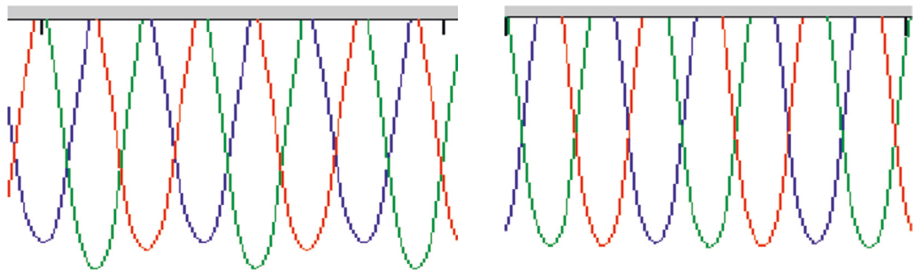

Figure 18: The AC voltage contrast of two different inverter sides after amplification.

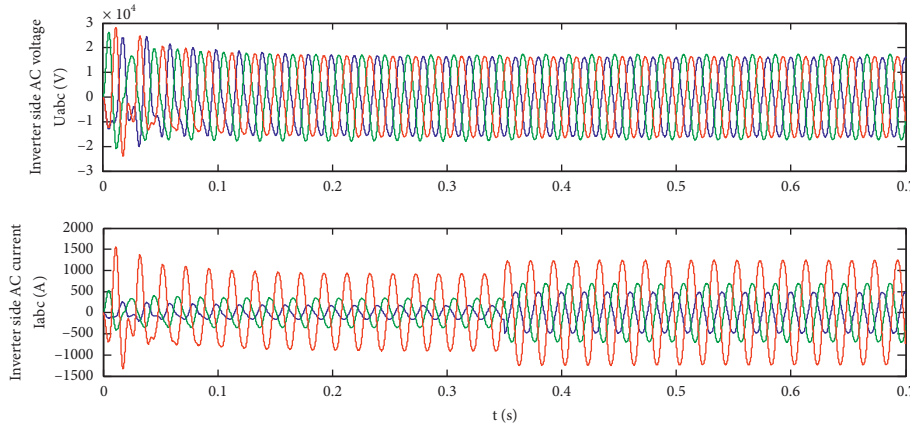

Figure 19: Simulation results of the common inverter side with load changing at 0.35s.

voltage. The simulation results in SIMULINK are shown in Figures 16–18.

Figure 16 shows the three-phase voltage and current wave forms obtained by the conventional constant voltage single-loop control when the inverter supplies power to the three-phase asymmetric load. It can be seen from the waveform that the three-phase voltage has asymmetrical distortion. In addition, the three-phase voltage waveform contains a large number of harmonic components.

Figure 17 shows the voltage and current simulation wave forms after the double closed-loop control and PR control of the "outer loop fixed AC voltage-inner loop current decoupling," when the inverter is powered by the three-phase asymmetric load. It can be concluded from the figure that the AC output voltage on the inverter side remains basically unchanged after 0.1 s. After 0.1 s, although the phase of the three-phase current is asymmetrical, the magnitude of the current remains substantially constant and

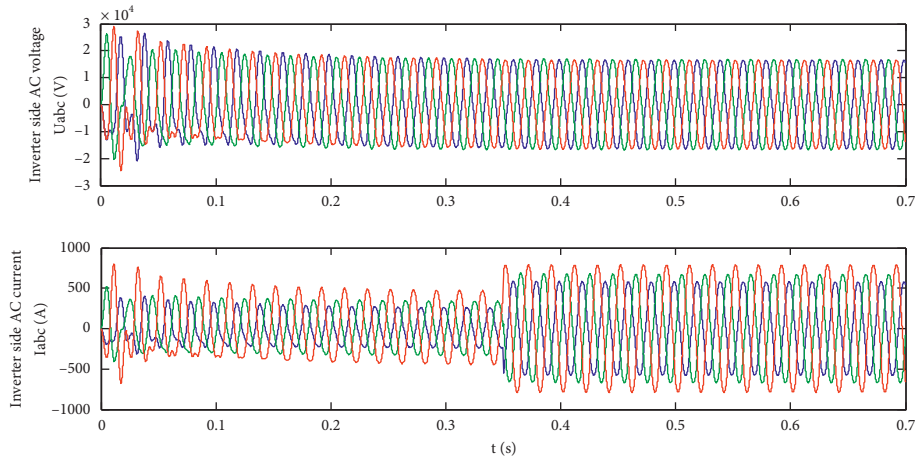

Figure 20: Simulation results of the improved inverter side with load changing at 0.35s.

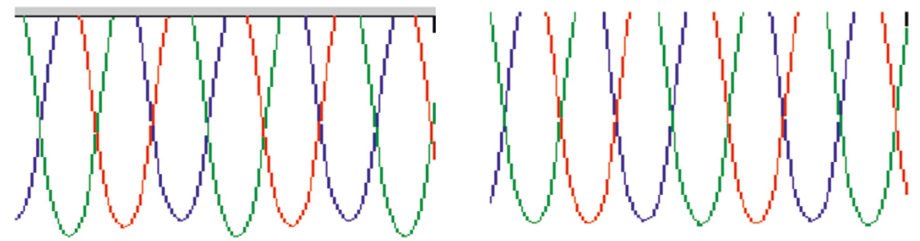

Figure 21: The AC voltage contrast of two different inverter sides after amplification.

the harmonics are greatly reduced. Under these circumstances, the stable of power is guaranteed.

Comparing Figures 16 and 17, it can be seen that the improved voltage outer loop control can solve the imbalance problem of the three-phase AC voltage under the three-phase asymmetric load and complete the voltage three-phase symmetry. In addition, by combining the inner loop current d/q decoupling control, the stabilization of the alternating voltage is achieved, and the harmonic content of the alternating voltage is reduced.

In order to further analyze the control performance of the "outer loop fixed AC voltage-inner loop current decoupling" double closed-loop control and PR control, a three-phase asymmetric loads of a, b, and c are 84 Ω, 50 Ω, and 24 Ω are simulated in the SIMULINK environment (Figure 19, Figure 20, and Figure 21).

Comparing Figures 19 and 20, it can be seen that the three-phase asymmetric load changes at 0.35s, the conventional fixed AC voltage control strategy loses its effectiveness, not only the three-phase AC voltage is distorted but also the three-phase AC current is distorted. After adopting the "outer loop fixed AC voltage-inner loop current decoupling" double closed-loop control and PR control, even if the three-phase asymmetric load changes at 0.35s, the three-phase AC voltage can maintain three-phase symmetry and amplitude stability. The control target of the "fixed AC voltage" on the inverter side is realized.

5. Conclusion

Based on the optimal control strategy of back-to-back converter, this article takes the traditional control strategy of back-to-back converter supplying to passive network as the starting point. And according to the actual situation of back-to-back converter supplying power to three-phase asymmetric passive network, this article analyzes the control objectives of the rectifier side and the inverter side of back-to-back converter, respectively.

For the rectifier side converter, the main purpose is to achieve a constant DC voltage. A double closed-loop control strategy of "fixed DC voltage-inner loop current decoupling" is designed. Optimize the voltage outer loop with fuzzy PI control. Optimize the current inner loop with PR control. The system reaction time and error overshoot are reduced, the d/p current coupling term is eliminated, and the anti-interference ability of the system is greatly improved.

For the inverter side converter, the double closed-loop control strategy of "fixed AC voltage-internal loop current decoupling" is designed to achieve the fixed AC voltage output as the control target. PR controller can perform the characteristics of no static tracking on a certain frequency signal and optimize the external loop constant voltage control, not only realizes the stable output of the fixed AC voltage but also greatly reduces the harmonic content of the AC voltage. The proposed method can solve the problem of

three-phase output voltage distortion when back-to-back converter is supplied to the three-phase asymmetric load and realizes the three-phase balance and stability of the AC output voltage.

The innovation points proposed in this article have certain guiding significance for the optimization of control strategy of back-to-back converter, the symmetrical fault ride through of converter supplying to three-phase asymmetric passive network, and the participation of back-to-back converter in the black start process of power grid.

Data Availability

The data that support the findings of this study are available from the corresponding author upon reasonable request.

Conflicts of Interest

The authors declare that there are no conflicts of interest regarding the publication of this article.

Acknowledgments

This research was funded by scientific research project of Shanghai Investigation, Design & Research Institute Co., Ltd (2021QT(831)-001).

References

[1] A. Egea-Alvarez, S. Fekriasl, and O. Hassan, "Advanced vector control for voltage source converters connected to weak grids," *IEEE Transactions on Power Systems*, vol. 30, no. 6, pp. 3072–3081, 2015.

[2] Z. Liu, J. Liu, and Y. Zhao, "A unified control strategy for three-phase inverter in distributed generation," *IEEE Transactions on Power Electronics*, vol. 29, no. 3, pp. 1176–1191, 2014.

[3] N. T. Navod, S. Rohan, M. K. Kagita, S. Lanka, and H. Ahmad, "Smart grid: a survey of architectural elements, machine learning and deep learning applications and future directions," *Journal of Intelligent Systems and Internet of Things*, vol. 3, no. 1, pp. 32–42, 2021.

[4] I. Nutkani, P. C. Loh, and F. Blaabjerg, "Droop scheme with consideration of operating costs," *IEEE Transactions on Power Electronics*, vol. 29, no. 3, pp. 1047–1052, 2014.

[5] M. Mullai, "Said broumi dominating energy in neutrosophic graphs," *International Journal of Neutrosophic Science*, vol. 5, no. 1, pp. 38–58, 2020.

[6] H. Laing, D. Yue, and D. Cao, "Research on VSC-HVDC double closed loop controller based on variable universe PID control," in *Proceedings of the 2017ChinaInternational Electrical and Energy Conference (CIEEC)*, vol. 633-8, Beijing, China, October 2017.

[7] G. Li, M. Guopeng, and C. Zhao, "Research of nonlinear control strategy for VSC- HVDC system based on Lyapunov stability theory," in *Proceedings of theThird International Conference on Electric Utility Deregulation and Restructuring and Power Technologies*, Nanjing, China, April 2008.

[8] L. i. Guangkai, L. i. Gengyin, H. Liang, C. Zhao, and M. Yin, "Research on dynamic characteristics of VSC-HVDC system," in *Proceedings of the IEEE Power Engineering Society General Meeting*, vol. 5, Montreal, Canada, June 2006.

[9] C. Xia, Y. Liu, K. Lin, and G. Xie, "Model and frequency control for three-phase wireless power transfer system," *Mathematical Problems in Engineering*, vol. 2016, Article ID 3853146, 9 pages, 2016.

[10] X. Yang, L . Zhu, and Z. Zhang, *Electric vehicles charging and discharging control strategy based on independent DC microgrid* in *Proceedings of the IEEE 3rd Advanced Information Technology, Electronic and Automation Control Conference (IAEAC)*, vol. 969-73, Chongqing, China, October 2018.

[11] M. Tian and F. Zhao, "Design principle and variant structure of a controllable reactor of transformer type," in *Proceedings of the Eighth International Conference on Electrical Machines and Systems*, vol. v3, pp. 1780–1783, Nanjing, China, September 2005.

[12] R. Eriksson, J. Beerten, M. Ghandhari, and R. Belmans, "Optimizing DC voltage droop settings for AC/DC system interactions," *IEEE Transactions on Power Delivery*, vol. 29, no. 1, pp. 362–369, Feb. 2014.

[13] J. Beerten and R. Belmans, "Analysis of power sharing and voltage devi-ations in droop-controlled DC grids," *IEEE Transactions on Power Systems*, vol. 28, no. 4, pp. 4588–4597, 2013.

[14] W. Y. Wang and M. Barnes, "Power flow algorithms for multi-terminal VSC-HVDC with droop control," *IEEE Transactions on Power Systems*, vol. 29, no. 4, pp. 1721–1730, 2014.

[15] C. Komathi and M. G. Umamaheswari, "Analysis and design of genetic algorithm-based cascade control strategy for improving the dynamic performance of interleaved DC–DC SEPIC PFC converter," *Neural Computing & Applications*, vol. 32, pp. 5033–5047, 2020.

[16] W. Lijuan, W. Haotian, and L. Xuesong, "Improvement on the grid connected control strategy of direct drive permanent magnet wind power system," in *Proceedings of the 26th Chinese Control and Decision Conference (2014 CCDC)*, pp. 4781–4785, IEEE, Kuala Lumpur, Malaysia, August 2014.

[17] L. Xu, L. l. Fan, and Z. Miao, "Modeling and simulation of multi-terminal HVDC for wind power delivery," in *Proceedings of the IEEE Power Electronics and Machines in Wind Applications*, pp. 1–6, Denver, CO, USA, July 2012.

[18] C. Dickensian, K. Srivastava, M. Reza, S. Cole, J. Beerten, and R. Belmans, "A distributed DC voltage control method for VSC–MTDC systems," *Electric Power Systems Research*, vol. 82, pp. 54–58, 2012.

[19] Z. QingChang and Z. Yu, "Control of inverters via a virtual capacitor to achieve captive output impedance," *IEEE Transactions on Power Systems*, vol. 29, no. 10, pp. 5568–5577, 2014.